Nonequilibrium molecular dynamics simulation of rapid directional solidification

Franck Celestini* and Jean-Marc Debierre

*Laboratoire Matériaux et Microélectronique de Provence, CNRS UMR 6137, Université d'Aix-Marseille III,
Faculté des Sciences et Techniques de Saint-Jérôme, Case 151, 13397 Marseille Cedex 20, France*

We present the results of nonequilibrium molecular dynamics simulations for the growth of a solid binary alloy from its liquid phase. The regime of high pulling velocities V, for which there is a progressive transition from solute segregation to solute trapping, is considered. In the segregation regime, we recover the exponential form of the concentration profile within the liquid phase. Solute trapping is shown to settle in progressively as V is increased and our results are in good agreement with the theoretical predictions of Aziz [J. Appl. Phys. **53**, 1158 (1981)]. In addition, the fluid advection velocity is shown to remain directly proportional to V, even at the highest velocities considered here ($V \simeq 10$ ms^{-1}).

I. INTRODUCTION

Directional solidification (DS) of binary alloys is a reference experimental method to conduct carefully controlled tests of industrial casting. Besides their practical interest, DS experiments also bring insight into the fundamental study of basic instability morphologies of solid-liquid interfaces, such as cells or dendrites.[1] By the combination of theoretical and numerical methods, much progress has been now achieved toward solving this difficult physical problem. However, most of the theoretical effort has concentrated so far on continuous descriptions of the underlying phenomena.[2] In contrast, attempts to attack the problem at the atomistic level remain very few. To this extent, the present study may be considered as a contribution to bridge the gap between both points of view.

Because of the micrometer size of the growth structures, a direct and quantitative atomistic simulation is still not at hand on this scale. Nevertheless, in the limit of large pulling velocities, a microscopic technique like molecular dynamics (MD) can still be used to follow atomistic phenomena occuring close to the solid-liquid interface. On one hand, MD was used to simulate laser-pulsed melting, for which the velocity is not controlled, but rather governed by heat diffusion.[3–6] On the other hand, a first MD simulation of directed growth has been recently reported by Coura and *et al.*[7] They considered the growth of a solid from a fluid phase with a density ten times smaller, a case which is probably more relevant to deposition from a vapor.

In this paper, we present nonequilibrium moleculardynamics simulations of directional solidification in two dimensions. We restrict ourselves to the case of rapid solidification with a large temperature gradient, for which the interface remains planar on the atomistic scale, so that microstructures will not be considered here. After the description of the simulation details in Sec. II, we present in Sec. III the results obtained for the segregation profiles, the segregation coefficient, and the advection velocity. In the last section, we finally discuss how this nonequilibrium simulation can be extended in the future to study different microscopic mechanisms involved in DS.

II. SIMULATION DETAILS

Two atoms i and j separated by a distance r interact via the well-known Lennard-Jones potential:

$$u_{ij}(r) = 4\epsilon_{ij}\left[\left(\frac{\sigma_{ij}}{r}\right)^{12} - \left(\frac{\sigma_{ij}}{r}\right)^{6}\right]. \quad (1)$$

The interaction energies between pairs of solvent-solvent, solute-solute, and solvent-solute atoms are, respectively, denoted by u_{11}, u_{22}, and u_{12}. The solvent potential parameters are chosen in order to describe argon properties ($\epsilon_{11} = 120$ K, $\sigma_{11} = 3.405$ Å). For the solute, we take $\epsilon_{22} = 0.5\epsilon_{11}$ and $\sigma_{22} = \sigma_{11}$. The cross-species parameters are fixed using the Lorentz-Berthelot rules[8]

$$\epsilon_{12} = \sqrt{\epsilon_{11}\epsilon_{22}} \quad (2)$$

and

$$\sigma_{12} = (\sigma_{11} + \sigma_{22})/2. \quad (3)$$

All the interactions are truncated at a cutoff radius $r_c = 2.5\sigma_{11}$ and the equations of motion are integrated using the Beeman algorithm[9] with a time step $\delta t = 0.01$ ps. The particle coordinates are defined in a reference frame moving at the pulling velocity V in the x direction and periodic boundary conditions (PBC's) are applied in the x and y directions. After integration of the dynamical equations over a time δt, pulling is implemented by adding an increment $-V\delta t$ to the x coordinate of each atom. In the reference frame, the solid-liquid interface is thus immobile when the stationary state is reached.

To simulate heat transport from the furnace to the system, four regions of fixed temperature are used (Fig. 1). Regions I, II, III, and IV are centered at fixed positions, x_I, x_{II}, x_{III}, and x_{IV} and have a width of 20 Å for regions I and IV and 10 Å for regions II and III. In each region the temperature is kept constant by using a classical velocity rescaling. To maintain the solidification front between regions II and III, we impose $T_I = T_{II} < T_m$ and $T_{III} = T_{IV} > T_m$, T_m being the melting temperature of the alloy.

In Fig. 1 we represent the temperature gradient obtained after equilibration in the simulation box. The large difference between T_{II} and T_{III} and hence the large gradient permits to

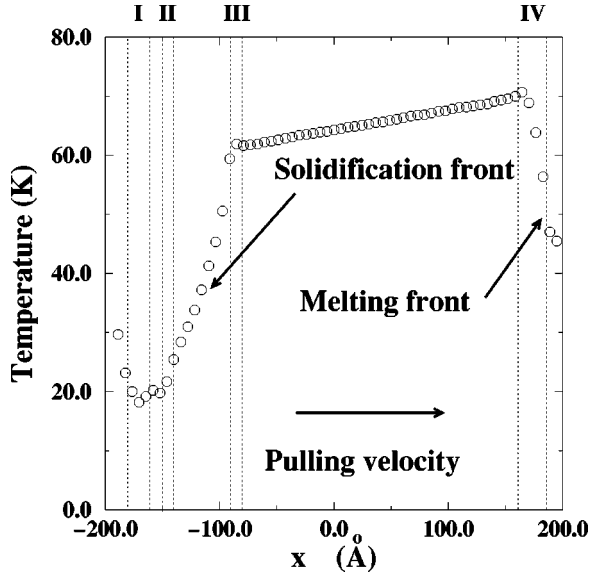PRB <u>62</u>   14 006

FIG. 1. Temperature profile along the x axis. The different regions of the simulation box in which the temperature is kept fixed are bounded by the dotted lines. The melting temperature is $T_m \simeq 40$ K.

localize the interface easily. With such a high gradient, instabilities cannot develop, which ensures the stability of planar interfaces. For the same reason we also take a small width L_y for the simulation box in order to reduce the natural roughness of the interface. More realistic systems, as compared to experiments, would correspond to $x_I = x_{II}$ and $x_{III} = x_{IV}$, together with a larger value of L_y. Because of the PBC in the x direction, we simultaneously have a solidification and a melting front, as in a zone melting experiment. We concentrate here on the solidification front and we use a wide liquid zone ($x_{III} < x < x_{IV}$) to allow solute diffusion. Fixing the temperature in four regions instead of two reduces considerably the rescaling of velocities within the liquid region. This is helpful to suppress perturbations and artifacts during the computation of microscopic quantities. The density difference between the solid and the liquid ($\simeq 20\%$) is sufficient to induce advection of the liquid towards the front. A part of the associated momentum is then transmitted to the solid layer which in turn acquires a translational motion in the x direction. To avoid this finite-size effect, we rescale to zero the mean velocity within the deeper part of the solid (region I).

Our system contains about 2000 atoms, 10% of which are solute atoms. Its size, $L_x = 400$ Å in length and $L_y = 60$ Å in width, is relatively modest as compared to the size of systems currently used in MD. The reason is that the computational effort is here essentially spent in the time length of the simulation. To obtain good statistics, the simulation has to be long enough to allow each atom to perform several solidification-melting cycles. Since ten cycles require a time of $10 L_x / V$, for the slowest velocity studied here ($V = 10$ cm s^{-1}), this represents a simulation time of 4×10^{-4} s (4×10^8 MD steps). To increase the performance of our code we then adopt the ''cell lists'' method[10] in which the box is divided into cells with a size slightly larger than the cutoff radius r_c.
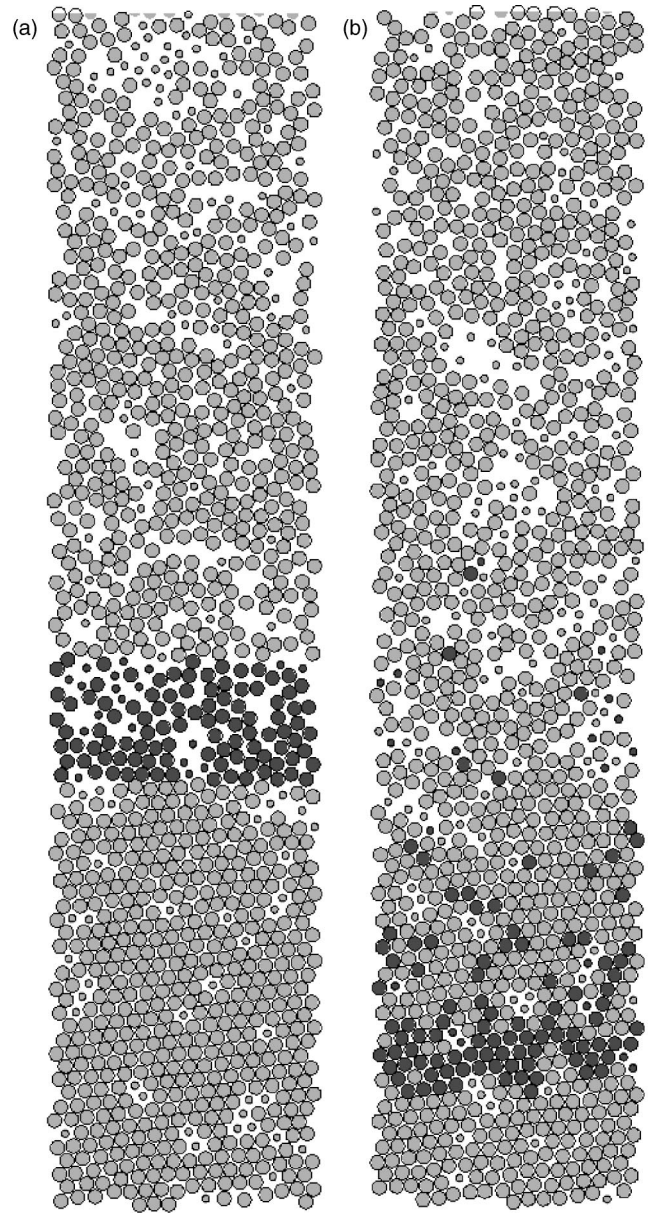

FIG. 2. Snapshots of the system at two different times ($V = 1$ ms^{-1}). Large and small radius, respectively, correspond to solvent and solute atoms (note that this is just a way to graphically distinguish between them; in the simulations $\sigma_{11} = \sigma_{22}$). (a) At $t = 0$, solute atoms are randomly placed in the simulation box. One slice of liquid in contact with the interface is marked (dark grey). (b) At time $t = 5$ ns, almost all the solvent atoms have solidified while a majority of the solute atoms remained liquid.

III. RESULTS

A. Concentration profiles

The partition ratio, or segregation coefficient, is defined as

$$k = c_s^i / c_l^i, \qquad (4)$$

c_l^i and c_s^i being the concentrations at the interface, respectively, in the liquid and the solid. With our choice of the potential parameters ($\epsilon_{12} < \epsilon_{11}$), k is expected to be less than one,[11] so that solute accumulates in the liquid near the front. We first illustrate how the simulation reproduces solute
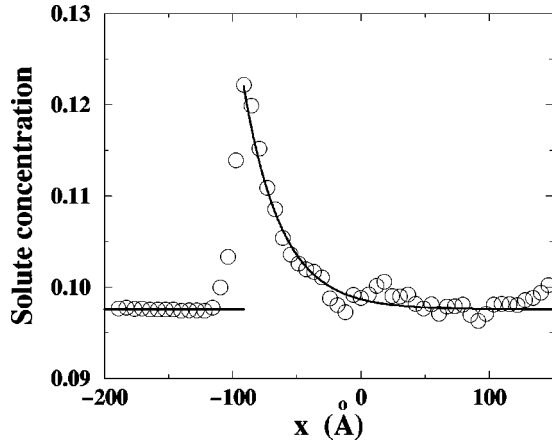
FIG. 3. Concentration profile $c(x)$ along the pulling direction, perpendicular to the interface ($V=1$ ms^{-1}).

rejection. The pulling velocity is fixed to $V=1$ ms^{-1} and the solute atoms are initially placed at random in the simulation box. Figure 2(a) is a snapshot of the system in its initial configuration. After a time $\Delta t=5$ ns, which corresponds to a spatial translation of the furnace of approximately $L_x/8$, the second snapshot [Fig. 2(b)] shows that almost all the solvent atoms initially close to the front are incorporated into the solid. Conversely, because of their poorer solubility in the solid phase, a majority of the solute atoms remain in the liquid phase. As compared to a solvent atom, it takes a longer time for a solute atom to cross the interface and hence the solute concentration is higher at the interface, as expected here. To quantify this segregation, we compute the profile concentration by averaging over 10^4 uncorrelated spatial configurations (Fig. 3). The diffusion equation for the solute in the moving frame reads

$$\frac{\partial c}{\partial t}=D\frac{\partial^2 c}{\partial x^2}+V\frac{\partial c}{\partial x}. \tag{5}$$

In the stationary regime, it gives the well-known theoretical profile for the solute concentration in the liquid,

$$c(x)=c_s^i+(c_l^i-c_s^i)\exp(-x/l_s), \tag{6}$$

where $l_s=D/V$ is the diffusion length and the origin of the x axis is placed at the front. A good agreement is found between this expression and our simulations, the best fit giving a diffusion coefficient $D_{fit}=0.3$ Å^2 ps^{-1}. To verify this value, we independently compute the diffusion coefficient profile $D(x)$, with the help of Einstein's relation between the mean-square displacement of the atoms and D,

$$\langle|\mathbf{r}(0)-\mathbf{r}(t)|^2\rangle=4Dt. \tag{7}$$

In Fig. 4, we see that the diffusion coefficient increases abruptly between zero in the solid phase to roughly 0.4 Å^2 ps^{-1} in the liquid near the interface. This variation of D takes place over a distance of 30 Å that can be considered as a good approximation of the interface width. In Eq. (5), D was assumed constant. We can check that the fitted value D_{fit} approximately corresponds to the average of $D(x)$ within the liquid region near the interface. The same analysis is repeated for different pulling velocities between V
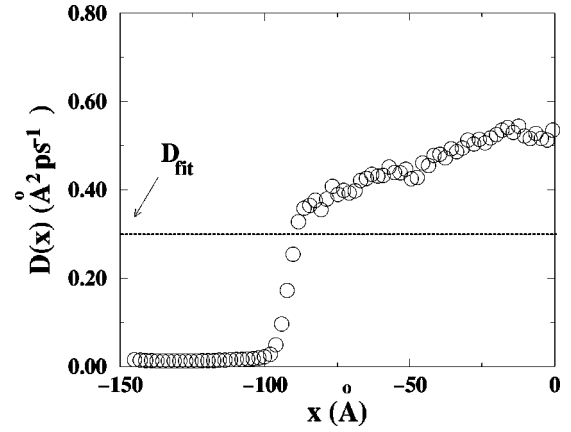

FIG. 4. Diffusion profile $D(x)$ along the direction perpendicular to the interface ($V=1$ ms^{-1}). The horizontal dotted line is the average diffusion coefficient obtained by fitting the concentration profile of Fig. 3 to an exponential law.

$=0.1$ ms^{-1} and $V=5$ ms^{-1}. For each velocity, we compute the concentration profile and extract D_{fit} from the diffusion length. In Fig. 5, D_{fit} is plotted as a function of the pulling velocity. As discussed below, the segregation coefficient tends to unity for the largest V and the calculation of D_{fit} is thus restricted to velocities $V<3$ ms^{-1}. A reasonable agreement is found in each case between D_{fit} and the average value of the $D(x)$ profile.

In Fig. 6, we plot the two concentration profiles obtained for $V=1$ ms^{-1} and $V=0.5$ ms^{-1}. As expected, the smaller the velocity, the larger l_s. If the agreement with the exponential law is good for the largest velocity, we notice that it is less satisfactory for the smaller one. This can be understood by a second look at Fig. 4. We observe that the thermal gradient induces an increase of the diffusion coefficient, as we go deeper in the liquid. As a consequence, we also have an increase of the diffusion length, which explains the disagreement observed for the largest x values.

B. Segregation coefficient

Now that we verified the ability of our method to reproduce both the segregation at the interface and the dependence of the diffusion length on the pulling velocity, we examine
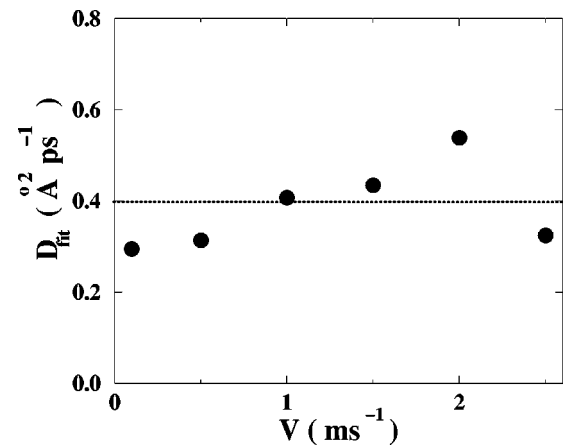

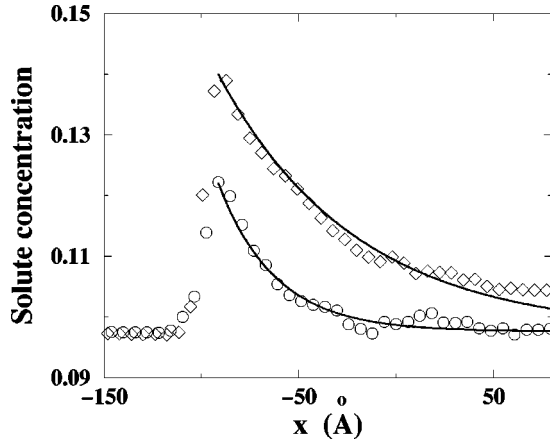FIG. 5. The average diffusion coefficient as a function of the pulling velocity.

FIG. 6. Solute concentration profiles obtained for $V = 1$ ms^{-1} (circles) and $V = 0.5$ ms^{-1} (diamonds). The continuous lines are best fits to Eq. (6).

the behavior of the segregation coefficient k as a function of V. We see in Fig. 6 that the liquid concentration at the interface, c_l^i, is larger for a lower value of V. This can be easily explained by the fact that, at large pulling velocities, the solute does not have enough time to fully diffuse over the interface width before it is incorporated into the solid. As a consequence, some solute is trapped in the solid and segregation at the interface is lowered. Several models have been proposed to describe solute trapping.[12–15] The usual qualitative criterion for segregation is to compare two different characteristic times. One, $t_V = \delta_i / V$, corresponds to the growth of the solid over a distance comparable to the interface width, δ_i. The second, $t_D = \delta_i^2 / D$, is the time needed for a solute atom to diffuse over the same distance δ_i. The Aziz model[12] predicts then

$$k = \frac{k_e + \beta}{1 + \beta} \qquad (8)$$

for the segregation coefficient. Here k_e is the segregation coefficient at equilibrium (i.e., when $V = 0$) and

$$\beta = t_D / t_V = \delta_i / l_s \qquad (9)$$

is the ratio of the two characteristic times (or lengths) defined above. Two remarks arise at this point. The first one concerns the neighborhood of the absolute stability threshold, $V = V_a$, where the diffusion length becomes comparable to the capillary length, $l_s \simeq d_0$. When $d_0 \gg \delta_i$, one also has $\beta \ll 1$, so that $k \simeq k_e$. In this case, the absolute stability threshold is well described by the usual linear stability analysis (see Ref. 2). This is not true anymore, when d_0 becomes comparable to δ_i, as it is very likely the case for some reference alloys.[16] The second remark is that the assumption of continuous growth, on which Eq. (8) relies, is actually verified by the rough solid-liquid interfaces produced with our Lennard-Jones potential.

In Fig. 7 we plot our estimates for k as a function of the pulling velocity. The line is a best fit to the Aziz model. The parameter β is estimated by using $\delta_i = 30$ Å, the characteristic width of the interface extracted from the $D(x)$ profile in Fig. 4 and the value of the diffusion coefficient, $D = 0.2$ Å^2 ps^{-1} is estimated at the center of this interface
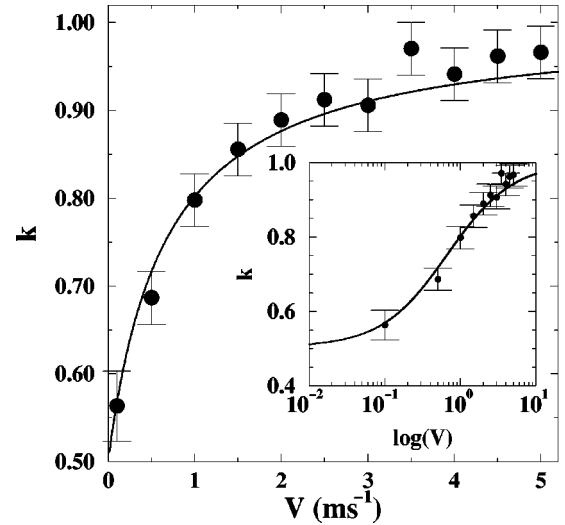

FIG. 7. Variations of the segration coefficient with the pulling velocity. The solid line is the best fit to the Aziz equation.

region. The agreement between the simulated values and the model is rather good for a fit with a single free parameter. We obtain the value $k_e = 0.503$ which is difficult to confirm because it is not possible to simulate segregation at much lower velocities with current computing power. Simulations at different pulling velocities thus provide an indirect way of determining k_e. The fact that the interface is moving permits all atoms, and especially the solute ones, to be part of the fluid phase and then to speed up relaxation to the equilibrium situation. For an immobile interface, one would have to wait for the very slow diffusion of solute atoms within the solid phase. The solid-liquid equilibrium for 3D binary Lennard-Jones mixtures has been determined by Monte Carlo simulations.[11,17] It would be interesting to have similar 2D results available to test our indirect evaluation of k_e.

C. Advection velocity

We finally study the advection of the fluid near the solidification front. The Lennard-Jones mixture considered in this work produces a substantial density difference between the solid and the liquid. This is illustrated in Fig. 8, where we
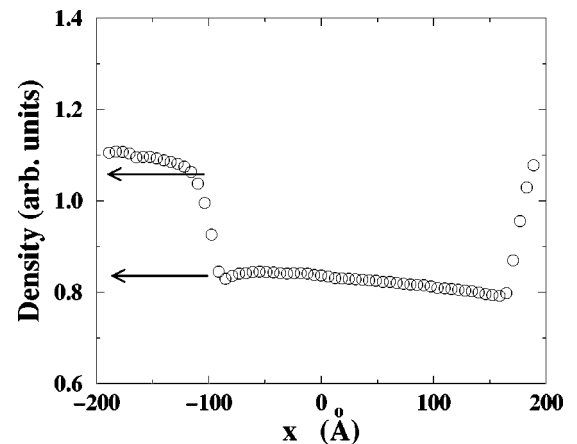

FIG. 8. Density profile $\rho(x)$ along the direction perpendicular to the interface ($V = 1$ ms^{-1}). The upper and lower arrows indicate respectively ρ_s^i and ρ_l^i at the solid-liquid interface.
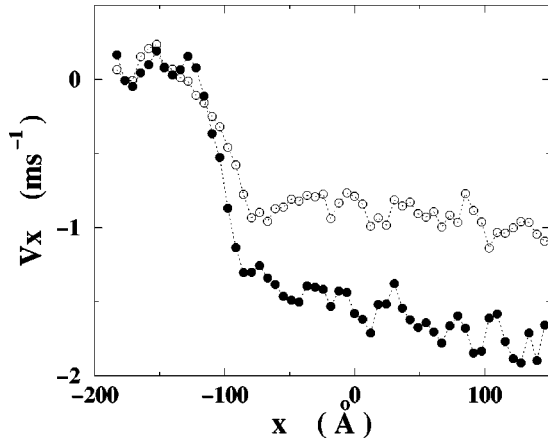
FIG. 9. Velocity profiles, $V_x(x)$, along the direction perpendicular to the interface. Open and filled circles, respectively, correspond to $V=3$ ms^{-1} and $V=5$ ms^{-1}.

FIG. 10. Interface advection velocity V_{ad}^i, plotted as a function of the pulling velocity V. The solid line corresponds to Eq. (10).

plot the density profile along the x direction perpendicular to the interface. From these data, we estimate both densities at the interface, ρ_s^i and ρ_l^i. We find that they do not depend on the pulling velocity and that the normalized density difference is also a constant, $(\rho_s^i - \rho_l^i)/\rho_l^i \simeq 0.24$. This rather high value for a Lennard-Jones potential is due to the large temperature gradient imposed at the interface. As a consequence, the solid cannot grow unless the liquid is advected toward the front with a velocity V_{ad}. In the laboratory frame, the solid is at rest, while the liquid has an advection velocity V_{ad} all along the x axis (Fig. 9). Mass conservation at the interface imposes that V_{ad}^i varies with V as

$$V_{ad}^i = \frac{\rho_s^i - \rho_l^i}{\rho_l^i} V. \qquad (10)$$

A linear variation is effectively recovered in our simulations (Fig. 10), with a slope comparing well to the estimate extracted from the density profile (see Fig. 8). It is interesting to note that there is no deviation from the linear law, even at the highest velocities studied in this work. On one side, one could have expected that the onset of solute trapping would modify the densities. This is not the case here, probably because the solvent and solute atoms have the same atomic radius, $\sigma_{22} = \sigma_{11}$. On the other side, a deviation would also appear as V is increased, if the solid was created with more and more defects. We would then have a decrease of V_{ad}^i because the density of the solid would also decrease. This type of deviation is not observed any more in our simulations. We finally see in Fig. 9 that the advection velocity increases in magnitude with x. As we go deeper in the liquid, the density progressively decreases in the thermal gradient and an extra advection velocity is thus necessary to compensate the density drop between two adjacent slices of alloy.

IV. CONCLUSIONS

With the help of MD simulations, we directly observed and analyzed quantitatively two important phenomena occur-
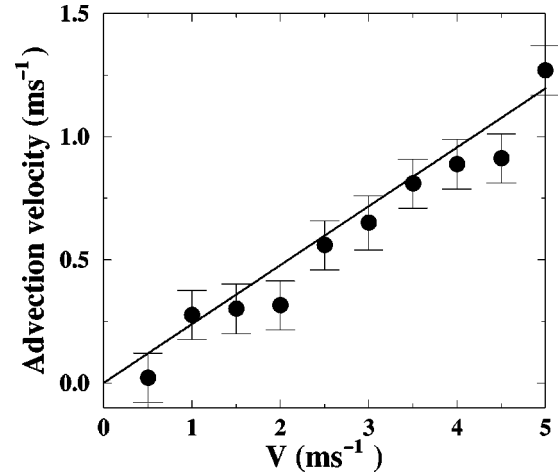
ring at the atomistic level in rapid DS. The first one is the crossover between the regime of solute segregation and the regime of solute trapping, which sets in as the pulling velocity V is increased. The good quantitative agreement of our estimates for the segregation coefficient, $k(V)$, with existing theories[12-14] confirmed that MD is a valuable simulation tool for DS. It would also be interesting in the future to test MD results against phase field models of solute trapping.[15] The second point is the advection of the liquid phase towards the solidification front. The advection velocity at the interface was shown to remain proportional to V, in the whole range of values considered here. This effect is more likely masked by a stronger phenomenon like convection in the usual experimental setups. It may, however, become relevant in microgravity or for thin sample DS. Finally, we observed no influence of the velocity on the interface temperature. Thus interface kinetic effects are probably very small in our system.

The use of Lennard-Jones potentials is rather restrictive to compare the present results with experiments. In the future, potentials based on empirical descriptions, like the glue model,[18] the embedded-atom method,[19] or the effective-medium theory[20] will be used to study technical materials like metals. This will allow us to explore important issues like anisotropy and faceting, or the role of defects and constraints. In parallel, it will be necessary to simulate more extended systems, in order to explore the front instabilities from an atomistic point of view. In this last category, we can cite the oscillations of the solidification front just above the absolute stability velocity.[21,22]

*Electronic address: celest@matop.u-3mrs.fr

[1] B. Billia and R. Trivedi, in *Handbook of Crystal Growth*, Vol. Ib, edited by D. T. J. Hurle (North-Holland, Amsterdam, 1993).

[2] K. Kassner, *Pattern Formation in Diffusion-Limited Crystal Growth* (World Scientific, Singapore, 1996).

[3] F. F. Abraham and J. Q. Broughton, Phys. Rev. Lett. **56**, 734 (1986).

[4] D. K. Chokappa, S. J. Cook, and P. Clancy, Phys. Rev. B **39**, 10 075 (1992).

[5] C. F. Richardson and P. Clancy, Phys. Rev. B **45**, 12 260 (1992).

[6] M. J. P. Nijmeijer and D. P. Landau, Comput. Mater. Sci. **1**, 389 (1993).

[7] P. Z. Coura, O. N. Mesquita, and B. V. Costa, Phys. Rev. B **59**, 3408 (1999).

[8] J. S. Rowlinson, in *Liquids and Liquids Mixtures* (Butterworth Scientific, London, 1982).

[9] D. Beeman, J. Comput. Phys. **20**, 130 (1976).

[10] D. Frenkel and B. Smit, *Understanding Molecular Simulation* (Academic, San Diego, London, 1996), p. 899.

[11] M. R. Hitchcock and C. K. Hall, J. Chem. Phys. **110**, 11 433 (1999).

[12] M. J. Aziz, J. Appl. Phys. **53**, 1158 (1981).

[13] R. F. Wood and G. E. Giles, Phys. Rev. B **23**, 2923 (1981); **23**, 5555 (1981); R. F. Wood *ibid.* **25**, 2786 (1982).

[14] J. W. Cahn, S. R. Coriell, and W. J. Boettinger, in *Laser and Electron Beam Processing of Materials*, edited by C. W. White and P. S. Peercy (Academic, New York, 1980).

[15] A. A. Wheeler, W. J. Boettinger, and G. B. McFadden, Phys. Rev. E **47**, 1893 (1993); N. A. Ahmad, A. A. Wheeler, W. J. Boettinger, and G. B. McFadden, *ibid.* **58**, 3436 (1998).

[16] For the succinonitrile-10% acetone alloy, the capillary length is about 3 Å.

[17] X. Cottin and P. A. Monson, J. Chem. Phys. **105**, 10 022 (1996).

[18] F. Ercolessi, M. Parrinello, and E. Tossati, Philos. Mag. A **58**, 213 (1988).

[19] M. S. Daw and M. I. Baskes, Phys. Rev. B **29**, 6443 (1984).

[20] K. W. Jacobsen, J. K. Nørskov, and M. J. Puska, Phys. Rev. B **35**, 7423 (1987).

[21] H. Müller-Krumbhaar and W. Kurz, *Solidification in Materials Science and Technology*, edited by R. W. Cahn, P. Haasen, and E. J. Kramer (VCH Verlagsgesellshaft, Weinheim, 1991), p. 55.

[22] A. Karma and A. Sakrissian, Phys. Rev. Lett. **68**, 2616 (1992); Phys. Rev. E **47**, 513 (1993).